

# Transient UV Raman Spectroscopy Finds No Crossing Barrier between the Peptide $\alpha$ -Helix and Fully Random Coil Conformation

Igor K. Lednev, Anton S. Karnoup, Mark C. Sparrow, and Sanford A. Asher\*

Contribution from the Department of Chemistry, University of Pittsburgh, Pittsburgh, Pennsylvania 15260

Received September 14, 2000. Revised Manuscript Received December 13, 2000

**Abstract:** Transient UV resonance Raman measurements excited within the amide  $\pi \rightarrow \pi^*$  transitions of a 21 unit  $\alpha$ -helical peptide has for the first time determined a lower bound for the unfolding rate of the last  $\alpha$ -helical turn to form a fully random coil peptide. A 3 ns  $T$ -jump is generated with 1.9  $\mu\text{m}$  laser pulses, which are absorbed by water. Subsequent 3 ns 204 nm UV pulses excite the amide Raman spectra at delay times between 3 ns and 1 ms, to monitor the peptide conformational evolution. We find  $\sim 180$  ns relaxation times which result in a rate constant of  $> 5 \times 10^6 \text{ s}^{-1}$  for unfolding of the last  $\alpha$ -helical turn. Our data are inconsistent with slow  $\alpha$ -helix nuclei melting.

## Introduction

Any theory of protein folding must be able to describe the submicrosecond dynamics of the formation and melting of  $\alpha$ -helices,  $\beta$ -sheets, turns, and disordered secondary structures.<sup>1</sup> These theories must also be able to describe the longer time dynamics associated with tertiary contact formation which is important in the stability of the native structure.<sup>2</sup> The rates of melting and propagation of the different secondary structure motifs are proposed to be fast; estimates based on activation barriers indicate subpicosecond melting and propagation of individual  $\alpha$ -helical residues, while modeling gives 10–100 ps time regimes as individual residues rapidly move on the Ramachandran surface.<sup>3</sup> Thus, theoretical studies suggest nanosecond to microsecond time scales for formation of long  $\alpha$ -helices.

Only recently has it become possible to experimentally measure the first stages of protein folding.<sup>4–7</sup> These measure-

ments of the earliest events in protein folding are providing valuable information about the rate-limiting steps and the energy landscape folding funnels that determine the actual folding dynamics.<sup>1</sup>

Significant progress has been made in modeling the equilibrium structure and thermodynamics of  $\alpha$ -helical peptide and protein segments, using approaches such as the zipper model, for example.<sup>8,9</sup> However, the ability of these models to predict dynamics has not yet been adequately tested due to the lack of experimental information on the fast stages of  $\alpha$ -helix folding and unfolding.

For example, the zipper model expects a nucleation bottleneck in the folding of a fully random coil peptide; the formation of the first helical turn confronts a relatively large entropic barrier that slows nucleation. The presence of a large nucleation barrier between the  $\alpha$ -helix and random coil conformations will result in an apparent two-state kinetic behavior; crossing this barrier becomes the bottleneck for both  $\alpha$ -helix formation and melting.<sup>7</sup> In contrast, more complex behavior is expected when the nucleation barrier is small, and the all or none two-state system (where each peptide molecule is either fully  $\alpha$ -helix or fully random coil) disappears.

Recent stopped flow deep UV CD studies of  $\alpha$ -helix formation in a polyalanine-based peptide by Clarke et al.<sup>10</sup> concluded that  $\alpha$ -helix nucleation takes place in the millisecond time scale. In addition, they also concluded that melting of the last  $\alpha$ -helical turn nucleus was also much slower than the rates of  $\alpha$ -helix propagation.

In the work here we examine the rates of  $\alpha$ -helix folding and unfolding in the nanosecond to millisecond time regime by using kinetic UV resonance Raman spectroscopy (UVRS). We directly monitored the kinetics of melting of an  $\alpha$ -helix peptide to a fully random coil peptide (in the nanosecond to

\* Author to whom correspondence should be addressed.

(1) (a) Wolynes, P. G.; Onuchic, J. N.; Thirumalai, D. *Science* **1995**, *267*, 1619–1620. (b) Dill, K. A.; Chan, H. S. *Nat. Struct. Biol.* **1997**, *4*, 10–19.

(2) Creighton, T. E., Ed. *Protein Folding*; W. H. Freeman and Company: New York, 1992.

(3) (a) Brooks, C. L., III *J. Phys. Chem.* **1996**, *100*, 2546–2549. (b) Barron, L. D.; Hecht, L.; Wilson, G. *Biochemistry* **1997**, *36*, 13143–13147.

(4) Williams, S.; Causgrove, T. P.; Gilmanshin, R.; Fang, K. S.; Callender, R. H.; Woodruff, W. H.; Dyer, R. B. *Biochemistry* **1996**, *35*, 691–697.

(5) (a) Phillips, C. M.; Mizutani, Y.; Hochstrasser, R. M. *Proc. Natl. Acad. Sci. U.S.A.* **1995**, *92*, 7292–7296. (b) Muñoz, V.; Thompson, P. A.; Hofrichter, J.; Eaton, W. A. *Nature* **1997**, *390*, 196–199. (c) Thompson, P. A.; Eaton, W. A.; Hofrichter, J. *Biochemistry* **1997**, *36*, 9200–9210. (d) Eaton, W. A.; Muñoz, V.; Thompson, P. A.; Henry, E. R.; Hofrichter, J. *Acc. Chem. Res.* **1998**, *31*, 745–753. (e) Dyer, R. B.; Gai, F.; Woodruff, W. H.; Gilmanshin, R.; Callender, R. H. *Acc. Chem. Res.* **1998**, *31*, 709–716. (f) Ballew, R. M.; Sabelko, J.; Gruebele, M. *Proc. Natl. Acad. Sci. U.S.A.* **1996**, *93*, 5759–5764. (g) Gruebele, M.; Sabelko, J.; Ballew, R. M.; Ervin, J. *Acc. Chem. Res.* **1998**, *31*, 699–707. (h) Crane, J. C.; Koepf, E. K.; Kelly, J. W.; Gruebele, M. *J. Mol. Biol.* **2000**, *298*, 283–292. (i) Yamamoto, K.; Mizutani, Y.; Kitagawa, T. *Biophys. J.* **2000**, *79*, 485–495.

(6) Lednev, I. K.; Karnoup, A. S.; Sparrow, M. C.; Asher, S. A. *J. Am. Chem. Soc.* **1999**, *121*, 8074–8086.

(7) Thompson, P. A.; Muñoz, V.; Jas, G. S.; Henry, E. R.; Eaton, W. A.; Hofrichter, J. *J. Phys. Chem. B* **2000**, *104*, 378–389.

(8) Cantor, C. R.; Schimmel, P. R. *The Behaviour of Biological Macromolecules*; Biophysical Chemistry; W. H. Freeman and Co.: San Francisco, 1980; Part III.

(9) Scholtz, J. M.; Qian, H.; York, E. J.; Stewart, J. M.; Baldwin, R. L. *Polymers* **1991**, *31*, 1463–1470.

(10) Clarke, D. T.; Doig, A. J.; Stapley, B. J.; Jones, G. R. *Proc. Natl. Acad. Sci. U.S.A.* **1999**, *96*, 7232–7237.

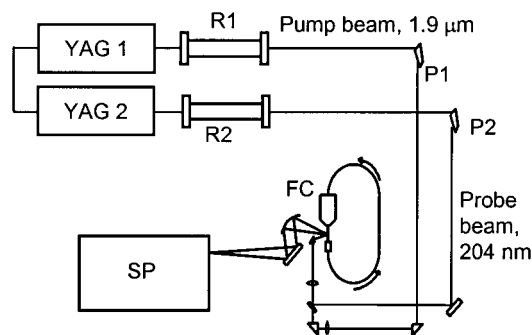


**Figure 1.** The  $T$ -jump spectrometer consists of two electronically synchronized Nd:YAG lasers, YAG 1 and YAG 2, two  $H_2$  Raman shifters, R1 and R2, a thermostated flow cell sample circulator, FC, and a Spex double monochromator with a blue enhanced ICCD detector, SP. The heating pump beam is obtained by Raman shifting the YAG 1 fundamental in  $H_2$  to  $1.9 \mu\text{m}$  (1-st Stokes). The probe beam is obtained by Raman shifting the YAG 2 third harmonic to 204 nm (fifth anti-Stokes). The time delays between the pump and probe pulses are computer controlled from  $\sim 3$  ns to  $\sim 1$  ms with  $\sim \pm 0.5$  ns accuracy.

microsecond time regime) and determined a lower bound for the unfolding rate of the last  $\alpha$ -helical turn ( $\alpha$ -helix nucleus melting). This work follows our earlier  $< 100$  ns studies of the  $T$ -jump unfolding of the 21 amino acid  $\alpha$ -helical peptide  $A_5$ -[AAARA] $_3$ A (AP).<sup>6,11</sup> Our work, as well as that of others<sup>4</sup> for similar peptides, has amply demonstrated that folding and unfolding occurs via two-state kinetics without any observable intermediates.

## Experimental Section

**$T$ -Jump Raman Spectral Measurements.** The studies here utilized a second generation nanosecond time-resolved UV Raman spectrometer for kinetic studies of protein folding initiated by a laser temperature jump (Figure 1). Our previous instrument utilized a single Nd:YAG laser both for generating the  $T$ -jump and for the UV Raman probe. This limited the longest possible delay time to  $\sim 100$  ns.<sup>6,11</sup> We now electronically synchronize two Coherent Inc., Infinity YAG lasers to obtain delay times between the 3 ns pump and probe pulses from  $\sim 3$  ns to  $\sim 6$  ms with a  $\sim \pm 0.5$  ns accuracy.

We Raman shifted the  $1.06 \mu\text{m}$  fundamental of a pump YAG laser to  $1.9 \mu\text{m}$  (1-st  $H_2$  Stokes shift) to selectively heat the water solvent (Figure 1). The magnitude of the  $T$ -jump was independently measured by using the  $\sim 3300 \text{ cm}^{-1}$   $H_2O$  and  $\sim 2500 \text{ cm}^{-1}$   $D_2O$  Raman bands, which show a large frequency and band shape temperature dependence.<sup>6,12</sup> We probed the peptide structural evolution by exciting the UV Raman amide spectra with delayed 204 nm UV pulses generated by the 5-th  $H_2$  antiStokes shifted frequency of a 3rd harmonic of the second Infinity YAG laser. The remainder of the Raman instrumentation has been described elsewhere.<sup>6</sup> Raman scattering was measured from the surface of a 0.6 mm diameter thermostatically controlled sample solution stream. The  $\sim 1$  ms upper delay time limit of our  $T$ -jump apparatus results from the sampling volume temperature jump decrease due to heat diffusion out of the sample volume irradiated by the heating pulse.<sup>4</sup>

The water ( $H_2O$ ) absorbance of 40/cm at  $1.9 \mu\text{m}$  decreases the IR beam intensity and the resulting  $T$ -jump 2.5-fold within the first 100  $\mu\text{m}$  sample thickness. To ensure that the Raman signal was obtained from the sample volume maximally heated by the IR pulse we adjusted the sample absorbance at 204 nm to be sufficiently large such that the resonance Raman light collected originates mainly from the sample stream surface.<sup>6</sup> Specifically, this requires the AP concentration as high

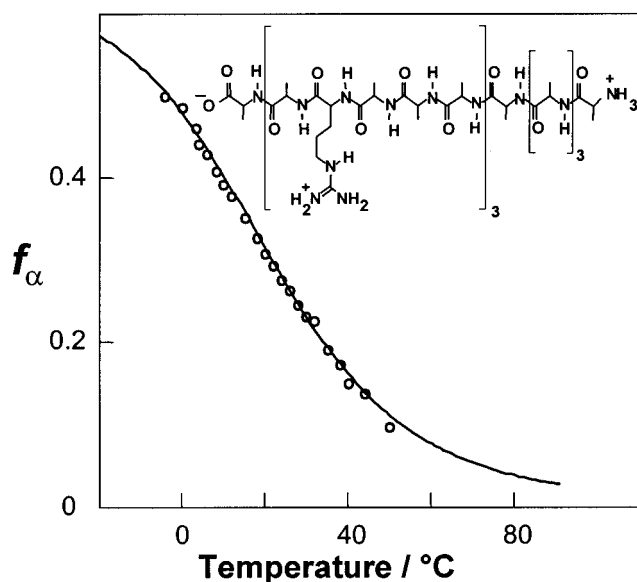


**Figure 2.** UVRS determined temperature dependence of the AP  $\alpha$ -helical fraction,  $f_\alpha$ . The solid line is the best fit to the zipper model (eqs 2, 3):  $f_{\text{end}} = 3.1 \pm 0.2$ ,  $\Delta h = -1.05 \pm 0.01 \text{ kcal/mol}$ ,  $\Delta s = -2.8 \pm 0.8 \text{ cal/(mol K)}$ ,  $\sigma = 8 \times 10^{-4}$ , and  $R^2 = 0.997$ . Inset: Molecular structure of AP.

as 15 mg/mL. To decrease the required AP concentration we also use  $D_2O$  as a solvent with 4.8/cm absorbance at  $1.9 \mu\text{m}$ .

The  $A_5(A_3RA)_3A$  peptide (AP) (95% purity) was prepared by the solid-phase peptide synthesis method at the Pittsburgh Cancer Institute.

## Results

**Random Coil  $\rightarrow$   $\alpha$ -Helix Transition Thermodynamics.** UVRS excited in the 200 nm spectral region selectively probes protein secondary structure,<sup>13,14</sup> because this excitation selectively enhances amide vibrations due to resonance with the amide backbone electronic transitions. These amide Raman bands sensitively depend on secondary structure. We recently determined the UVRS of the pure  $\alpha$ -helix,  $\beta$ -sheet, and random coil secondary structural motifs (PSSRS) of proteins and demonstrated that these PSSRS can be used to quantitatively determine protein secondary structure.<sup>14</sup>

We also determined the UVRS of the pure  $\alpha$ -helix and random coil conformations of the short alanine-based peptide AP.<sup>6</sup> The spectral differences between the AP basis spectra and the PSSRS spectra result from the fact that AP is almost an Ala oligopeptide. The AP Raman bands are narrow compared to those of the PSSRS due to the decreased inhomogeneous broadening associated with the distribution of protein amino acid residues.

We modeled the AP UV Raman equilibrium spectra observed at different temperatures as a linear combination of temperature-dependent AP pure random coil spectra and a pure  $\alpha$ -helix temperature independent spectrum.<sup>6</sup> As a result, we determined the temperature dependence of the fraction of  $\alpha$ -helix (Figure 2).

**AP transient UV Raman Spectra.** Figure 3a shows the time dependence of the UVRS spectral changes induced by a  $T$ -jump between 4 and 35  $^\circ\text{C}$  for AP in  $H_2O$ . The "infinite" time delay curves display the static UVR difference spectrum between AP at 4 and 35  $^\circ\text{C}$ . As shown in Figure 3a for AP in  $H_2O$ , the amide III band occurs between 1200 and 1300  $\text{cm}^{-1}$  while the

(11) Lednev, I. K.; Karnoup, A. S.; Sparrow, M. C.; Asher, S. A. *J. Am. Chem. Soc.* **1999**, *121*, 4076–4077.

(12) (a) Walrafen, G. E.; Fisher, M. R.; Hokmabadi, M. S.; Yang, W.-H. *J. Chem. Phys.* **1986**, *85*, 6970–6982. (b) Walrafen, G. E.; Yang, W.-H.; Chu, Y. C.; Hokmabadi, M. S. *J. Phys. Chem.* **1996**, *100*, 1381–1391.

(13) Song, S.; Asher, S. A. *J. Am. Chem. Soc.* **1989**, *111*, 4295–4305.

(14) Chi, Z.; Chen, X. G.; Holtz, J. S. W.; Asher, S. A. *Biochemistry* **1998**, *37*, 2854–2864.

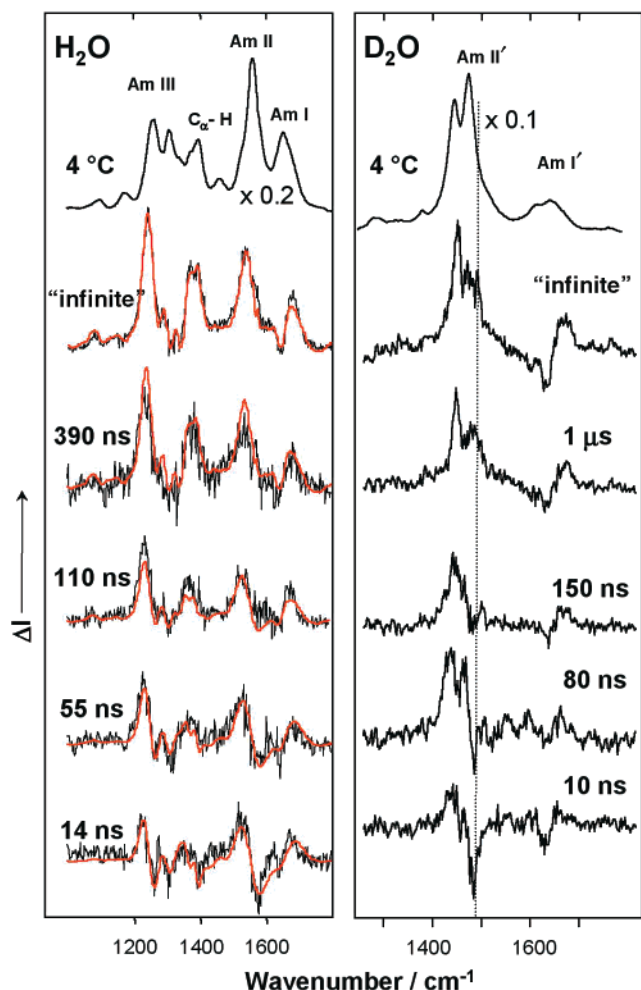


**Figure 3.** AP UVRS spectra (top curves) measured in H<sub>2</sub>O (D<sub>2</sub>O) solution at 4 °C and transient difference UVRS of AP in H<sub>2</sub>O (D<sub>2</sub>O) solution initially at 4 °C measured at different delay times after a *T*-jump of ~31 (~22) °C. The steady state difference UVRS spectrum between 35 (26) and 4 °C is the transient difference spectrum for an infinite delay time. Red curves: Transient spectra modeled with eq 1 by using pure  $\alpha$ -helix and random coil basis spectra and their measured temperature dependence with no free parameters.

C $\alpha$ -H symmetric bending band occurs at 1382 cm<sup>-1</sup> and the amide II and I bands occur at 1549 and 1643 cm<sup>-1</sup>. As discussed previously,<sup>6</sup> the difference spectral peaks at 1236, 1374, 1534, and 1678 cm<sup>-1</sup> are clearly due to an increased random coil conformation. At the shortest delay times, we only see features that derive from the known temperature downshifts of the Am II and Am III bands. We only observe random coil formation at longer delay times. At ~400 ns, the spectral evolution is complete and the difference spectrum becomes essentially identical to that which occurs at an infinite delay time. The spectral changes observed are associated with melting of the  $\alpha$ -helices to form random coil peptides. This conclusion is consistent with the IR study by Williams et al.<sup>4</sup> of a similar peptide, which also demonstrated evolution between only two species.

We also measured the *T*-jump kinetics for AP in D<sub>2</sub>O, which gives higher spectral signal-to-noise data that yield more accurate kinetic data. The amide N-deuterated AP spectrum shows an intense Am II' Raman doublet at 1446 and 1475 cm<sup>-1</sup>, which derives from the coupling of an almost pure C-N stretching vibration to a CH<sub>3</sub> asymmetric bending vibration.<sup>15</sup>

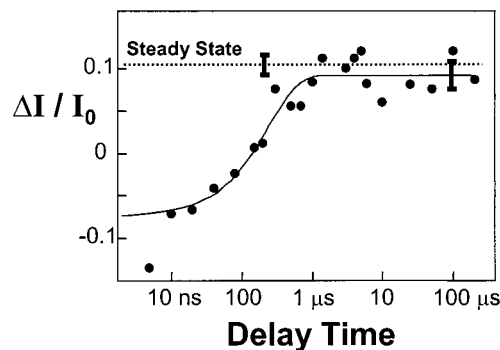


**Figure 4.** UVRS measured kinetics of AP thermal denaturation. Raman intensity data at 1487 cm<sup>-1</sup> were obtained from the difference transient UVRS measured for AP in D<sub>2</sub>O at different delay times and normalized to the 1476 cm<sup>-1</sup> band intensity of the 4 °C spectra. The best fit (solid curve,  $R^2 \approx 0.92$ ) to a monoexponential function with three free parameters, the relaxation rate constant (180 ns,  $2\sigma = 60$  ns), and the  $\Delta I / I_0$  at zero and infinite delay times was obtained by using the SPSS program. We did not utilize the shortest delay time (5 ns) data point in the analysis because it appears to result from an as yet uncharacterized very short time dynamics, which does not appear to be coupled to the longer time dynamics of the AP conformational changes. Also shown is the band intensity change for an infinite delay time obtained from the steady-state UVRS spectra measured at the initial and final *T*-jump temperatures. The data were obtained for a D<sub>2</sub>O solution of AP (~1 mg/mL). A detailed discussion of the D<sub>2</sub>O AP spectra will be presented elsewhere. The error bars (two standard deviations) represent a 95% confidence range for both the steady state and kinetic data.

The amide II' band has a much higher Raman intensity that results in higher spectral signal-to-noise ratios. In addition, D<sub>2</sub>O has a much lower absorptivity at the 1.9  $\mu$ m heating pulse (4.8/cm) than does H<sub>2</sub>O (40/cm). This allows us better control of the temperature jump and allows us to optimize the AP concentration for optimum spectral signal-to-noise ratios. Figure 3b shows the time dependence of the UVRS difference spectrum induced by a *T*-jump between 4 and 26 °C for AP in D<sub>2</sub>O. The doublet at 1451 and ~1475 derives from an increased random coil conformation.

We utilized the time dependence of the 1487 cm<sup>-1</sup> UVR difference band intensity to monitor the relaxation kinetics for a 22 °C *T*-jump for AP in D<sub>2</sub>O (Figure 4). Assuming monoexponential kinetics, we calculate a relaxation time of 180  $\pm$  60 ns, which agrees well with our earlier reported data for AP in H<sub>2</sub>O solution.<sup>6</sup>

## Discussion

**Modeling Transient Spectra.** We modeled the transient spectra using a linear combination of  $\alpha$ -helix and random coil steady-state basis spectra,  $\sigma_r$  and  $\sigma_\alpha$ , independently determined for the AP pure random coil and  $\alpha$ -helix conformations. The transient difference spectrum at any delay time *t* is

$$\Delta\sigma(t) = f_\alpha(0)[\sigma_\alpha(T_f) - \sigma_\alpha(T_i)] + [1 - f_\alpha(0)] \cdot [\sigma_r(T_f) - \sigma_r(T_i)] + [f_\alpha(t) - f_\alpha(0)] \cdot [\sigma_\alpha(T_f) - \sigma_r(T_f)] \quad (1)$$

where  $f_\alpha(0)$  and  $f_\alpha(t)$  are the fractional helicity at  $t = 0$  and at time *t* after the *T*-jump;  $T_i$  and  $T_f$  are the temperatures before and after the *T*-jump. The first two terms in eq 1 are due to the temperature-induced Raman spectral changes that occur within the  $\alpha$ -helix and random coil conformations in the absence of AP secondary structure changes. These terms are independent of the delay time *t*. They dominate the difference transient spectra at short delay times when the third term, which results from conformational transitions, is small.

We find that the  $\alpha$ -helix basis spectrum  $\sigma_\alpha$  is temperature independent, in contrast to the random coil basis spectra.<sup>6</sup> Consequently, the first term in eq 1 is negligible. The 14 ns delay time difference spectrum mainly results from the temperature dependence of the AP random coil spectrum (term 2 in eq 1) without significant contributions from conformational changes (term 3 in eq 1).

The conformational dependence of the amide UV Raman spectra of the polypeptide chain is mainly due to the changes in the Ramachandran  $\Phi$  and  $\Psi$  angles between the different conformations.<sup>16</sup> The temperature independence of the AP  $\alpha$ -helix spectra presumably results from the rigidity of the  $\alpha$ -helix conformation, whose  $\Phi$  and  $\Psi$  angles do not vary much with temperature. In contrast, the unordered random coil conformation has a distribution of  $\Phi$  and  $\Psi$  angles; this distribution varies with temperature.

We modeled the difference transient spectra assuming monoexponential kinetics for the fractional helicity  $f_\alpha(t) = f_\alpha(\infty) + [f_\alpha(0) - f_\alpha(\infty)] \cdot \exp(-t/t_0)$  with no free parameters ( $t_0 = 180$  ns). All of the Figure 3 modeled Raman difference spectra utilized the relaxation time,  $t_0$ , obtained from fits of the amide III,  $C_\alpha$ -H sb, amide II, and amide I difference band intensities to a monoexponential decay. Good agreement between the experimental and modeled difference spectra (Figure 3) indicates that the AP transient UVR spectra can be well described by the equilibrium basis spectra. This means that the transient intermediate at any delay time consists of pure helical and random coil conformations.

The small deviations of the Figure 3 fitted difference spectra compared to the measured difference spectra are likely due to small errors in the  $T$ -jump temperature, which derive from long time drifts in the average laser pulse energy. There is no indication of any new intermediate species since no new peaks appeared in the difference spectra. The small deviations observed (especially in the 110 and 390 ns data) appear to result from slightly decreased and increased difference bands due to these temperature errors. Repeated measurements indicate that the  $T$ -jump errors are randomly distributed.

As we previously demonstrated in our steady-state UVR study of AP helix melting,<sup>6</sup> the equilibrium spectra measured at different temperatures are well modeled as linear combinations of a temperature-dependent pure random coil spectrum and a temperature-independent pure  $\alpha$ -helix spectrum. This indicates a lack of any intermediates in the melting process of our alanine peptide. Keiderling and co-workers<sup>17</sup> recently characterized the temperature dependence of a similar Ala peptide using steady state vibrational circular dichroism (VCD). They argue that they detected an intermediate due to peptide conformations containing a mixed coil-helix structure. We see no evidence for this intermediate, possibly because our spectra result from the sum of contributions of individual Raman spectra of amide bonds, while the VCD spectra result from the coupling of a number of amide bonds.

The modeled transient spectrum obtained for the shortest (14 ns) delay time mainly results from a temperature-induced alteration of the spectrum of the AP random coil fraction. The good agreement of the 14 ns modeled spectrum with the experimental one (Figure 3) confirms again that the  $\alpha$ -helix UV Raman spectrum is essentially temperature independent.

**Nucleus Melting Kinetics.** Our  $T$ -jump kinetics are obviously dominated by a fast process with a relaxation time of  $\sim 180$  ns

(Figure 4). AP UVRS spectral changes initiated by a  $T$ -jump from 4 to 26 °C maximize in less than 1  $\mu$ s to difference spectra essentially identical to those observed in steady state measurements made at the initial and final  $T$ -jump temperatures (Figure 4). Thus, the thermal denaturation relaxation process is fully complete in  $\sim 1$   $\mu$ s.

The zipper model single sequence approximation appears to adequately describe the equilibrium helix-random coil thermal transition of short polypeptides.<sup>8,9</sup> We used well-known zipper model equations for calculating the partition function  $q$  and fractional helicity  $\theta_T$  assuming a temperature-independent nucleation parameter  $\sigma$  with a propagation equilibrium constant  $s = \exp(-\Delta H/RT + \Delta S/R)$ , where  $\Delta H$  and  $\Delta S$  are the enthalpy and entropy changes for a single propagation step and  $n$  is the helix length:<sup>8</sup>

$$q = 1 + \frac{\sigma s^2}{(s-1)^2} \left( s^n + \frac{n}{s} - n + 1 \right) \text{ and } \theta_T = \frac{s}{nq} \frac{\partial q}{\partial s} \quad (2)$$

We utilized the zipper model, recognizing that several terminal residues cannot effectively form fully  $\alpha$ -helix structures. Thus, we excluded these penultimate residues from the helix-random coil thermodynamic equilibrium by introducing the end effect factor  $f_{\text{end}}$  when calculating the AP fractional helicity,  $\theta$

$$\theta = \theta_T(1 - f_{\text{end}}) \quad (3)$$

where  $\theta_T$  is the theoretical fractional helicity of polypeptide (eq 2) that can be fully helical at low temperature.

We obtain an excellent Figure 2 fit of the zipper model to the AP steady-state melting curve ( $R^2 = 0.997$ ) and obtain the value  $f_{\text{end}} = 0.31 \pm 0.02$ , which is close to  $0.3 \pm 0.05$  that was previously estimated for AP using a two state model.<sup>6</sup> We obtain  $\Delta H = -1.05 \pm 0.01$  kcal/mol per residue, close to the ca.  $-1$  kcal/mol value previously found using CD and calorimetric measurements for ionizable polypeptides<sup>18,19</sup> (after correction for the heat of ionization of the side chains), and for Ala oligopeptides.<sup>9,20</sup> Our calculated  $\Delta S = -2.8 \pm 0.8$  cal/(mol K) compares well to the  $-3.4$  cal/(mol K) value reported for polyglutamic acid.<sup>19</sup> The nucleation parameter  $\sigma = 8 \times 10^{-4}$  was fixed for the fitting as reported for Ala-amino acid residues.<sup>8</sup>

Using these parameters we calculated the helical length distribution at 4 and 26 °C (Figure 5). The population of fully random coil AP molecules is calculated to increase from  $\sim 0.17$  to  $\sim 0.45$  between 4 and 26 °C, while the fractional helicity decreases from  $\sim 0.45$  to  $\sim 0.26$ .

These results directly contradict Clarke et al.'s<sup>10</sup> conclusion that  $\alpha$ -helix nucleus melting is slow, and that fully random coil AP molecules cannot form on microsecond time scales. Clark et al. would require that the entire decrease in the  $\alpha$ -helix content would solely result from partial melting of  $\alpha$ -helical segments without any crossing of the nucleation barrier.

Figure 5 shows the helical length distribution calculated for a kinetic intermediate system which is bottlenecked such that the population of fully random coil AP is fixed at the 4 °C equilibrium value. The remainder of the AP states, which contain helical segments, are calculated as if they were in thermodynamic equilibrium with each other at 26 °C as calculated from

(18) (a) Chou, P. Y.; Scheraga, H. A. *Biopolymers* **1971**, *10*, 657–680. (b) Rialdi, G.; Hermans, J. J. *J. Am. Chem. Soc.* **1966**, *88*, 5719–5720. (c) Scholtz, J. M.; Baldwin, R. L. *Annu. Rev. Biophys. Biomol. Struct.* **1992**, *21*, 95–118.

(19) Hermans, J. J. *J. Phys. Chem.* **1966**, *70*, 510–515.

(20) Scholtz, J. M.; Marqusee, S.; Baldwin, R. L.; York, E. J.; Stewart, J. M.; Santoro, M.; Bolen, D. W. *Proc. Natl. Acad. Sci. U.S.A.* **1991**, *88*, 2854–2858.

(16) (a) Krimm, S.; Bandekar, J. *Adv. Protein Chem.* **1986**, *38*, 183–364. (b) Lord, R. C. *Appl. Spectrosc.* **1977**, *31*, 187–194.

(17) Yoder, G.; Pancoska, P.; Keiderling, T. A. *Biochemistry* **1997**, *36*, 15123–15133.

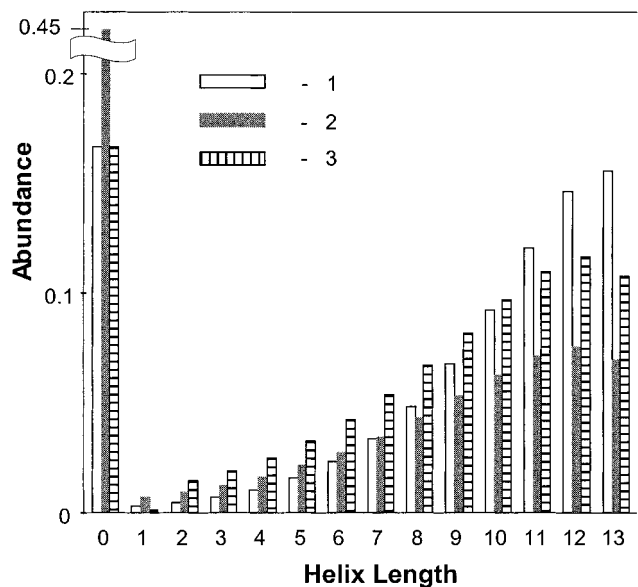


**Figure 5.** Distributions of helical lengths calculated by using the zipper model for AP in thermodynamic equilibrium at (1) initial and (2) final  $T$ -jump temperatures and (3) in a kinetic intermediate state where no fully random coil conformations can form (see text).

the zipper model. The fractional helicity of this kinetic intermediate at 26 °C is calculated to be  $\sim 0.39$ . Thus, only a

$-0.06$  decrease in fractional helicity could occur from the  $T$ -jump in  $\sim 1 \mu\text{s}$ . This is substantially smaller than the  $-0.19$  fractional helicity change observed in the  $1 \mu\text{s}$  kinetic measurements. This demonstrates that melting of the  $\alpha$ -helix peptides to fully random coil peptides occurs faster than  $1 \mu\text{s}$ . We see no evidence for slow melting of  $\alpha$ -helix nuclei.

Our conclusions are robust to variations of the thermodynamic parameters within reasonable limits. For example, little influence of the nucleation parameter value was found. For example, use of  $\sigma = 8 \times 10^{-3}$  gives a fractional helicity change of ca.  $-0.11$  for the formation of the kinetic intermediate at 26 °C, which is also too small.

Figure 4 clearly shows that the changes in the AP Raman spectra obtained  $\sim 1 \mu\text{s}$  after the  $T$ -jump are identical to those found between the steady-state spectra measured at the initial and final  $T$ -jump temperatures. We can calculate a lower bound for the rate of  $\alpha$ -helix nucleus melting required from the Figure 4 kinetics data. Within the spectral signal-to-noise ratios we find a rate constant  $> 0.5 \times 10^7 \text{ s}^{-1}$ . Thus, we find no evidence that melting of the  $\alpha$ -helix nucleus is a bottleneck for conversion of  $\alpha$ -helix peptides to fully random coil peptides.

**Acknowledgment.** We gratefully acknowledge NIH grant GM30741 for financial support.

JA003381P